








CuMoO₄@hexagonal boron nitride hybrid: an ecofriendly flame retardant for polyurethane elastomer

Wenzong Xu^{1,*} , Aijiao Li¹ , Yucheng Liu¹ , Rui Chen¹ , and Wu Li¹ 

¹ School of Materials Science and Chemical Engineering, Anhui Jianzhu University, 292 Ziyun Road, Hefei, Anhui 230601, People's Republic of China

Received: 31 January 2018

Accepted: 28 April 2018

Published online:

9 May 2018

© Springer Science+Business Media, LLC, part of Springer Nature 2018

ABSTRACT

A novel flame retardant (CuMoO₄@h-BN) was synthesized through the co-precipitation method, and its structure and morphology were systematically characterized. CuMoO₄@h-BN was added to polyurethane elastomer (PUE) to investigate the effect of thermal, flame retardancy and smoke suppression properties on the PUE composites. The results showed that 2 wt% CuMoO₄@h-BN increased the residual char yield of the PUE composite notably to 9.8%. CuMoO₄@h-BN exhibited an excellent charring effect. Compared with pure PUE, 2 wt% CuMoO₄@h-BN decreased the peak heat release rate, total heat release and smoke density of the PUE composite by 73.6, 52.4 and 28.2%, respectively. CuMoO₄@h-BN performed well in flame retardancy and smoke suppression. It may be attributed mainly to the physical barrier effect of h-BN and catalytic carbonization effect of CuMoO₄. It is expected that this simple and inexpensive treatment of PUE may help expand the fire safety applications of the material.

Introduction

With the rapid social and economic development, functional materials have become increasingly important. Particularly, flame-retarding polymers have attracted more and more interest, due to their wide application (such as in aerospace engineering, information technology, construction and textile) [1–3]. Numerous studies have shown that the flame retardancy of polymers can be improved by adding nano-inorganic flame retardants [4–6]. Therefore, the

development of nano-inorganic flame retardants is important for flame-retarding polymers.

Hexagonal boron nitride (h-BN) has a layered structure similar to graphite and is called “white graphite.” Each of its layers is composed of B atoms and N atoms. The B atoms and N atoms are covalently bonded by *sp*² hybrid to produce unlimited extension of hexagonal ring networks, and interlayers combined by the van der Waals forces. In addition, h-BN is widely used in machinery, metallurgy, electronics, aerospace and other high-tech fields, due to

Address correspondence to E-mail: wenzongxu@ahjzu.edu.cn

its excellent physical and chemical properties, such as high temperature resistance, oxidation resistance, chemical stability, low coefficient of friction and good processability [7–9]. Compared with carbon nanomaterials, boron nitride nanomaterials have better thermal stability, chemical stability and oxidation resistance. Therefore, h-BN has remarkable advantages in improving the mechanical properties, thermal stability and oxidation resistance of polymers. Yu et al. obtained BNO by calcination of h-BN and then added BNO to modified EP (MEP) to study the effect of flame retardancy on the BNO/MEP composite. They found that BNO exhibited good flame retardancy and that the incorporation of 1 wt% BNO reduced the PHRR by 47.2% [10]. Gu et al. chemically modified h-BN with hexachlorocyclotriphosphazene and p-phenylenediamine and added it to bis-maleimide resin to study the thermal and flame retardant properties of the composites. Their results showed that modified h-BN could effectively improve the thermal stability and flame retardancy of resin; the PHRR was reduced from 383 to 207 kW m⁻², down by 45.9% [11]. Qu et al. [12] found that PCB-BN synthesized by hexachlorocyclotriphosphazene, bisphenol-A and BN could effectively improve the flame retardancy of EP. Hexagonal boron nitride could improve the flame retardancy of the polymer due mainly to its good thermal stability and physical barrier effect.

As is known, polymers can produce a lot of toxic gas and smoke during the combustion process. In fact, these harmful volatile substances and smoke are the greatest threats to the safety of human life in a fire. Therefore, it is a major challenge to effectively reduce the generation of smoke for flame-retarding polymers. Numerous studies have shown that molybdenum-containing compounds and copper-containing compounds can well inhibit the generation of smoke during the combustion of polymers [13, 14]. Zhou et al. [15] found that putting layered double hydroxides (LDHs) on the surface of molybdenum disulfide (MoS₂) could not only effectively reduce the PHRR of EP, but also reduce the production of hydrocarbons, CO and CO₂, and effectively reduce the TSP during the combustion of EP. Xu et al. studied the application of MoO₃ and graphene in polyurethane elastomer. They found that MoO₃ and graphene hybrids exhibited good smoke suppression and that the incorporation of 2 wt% hybrids reduced the smoke density by 29.5%. That was because MoO₃

promoted the formation of a dense char layer during the combustion of the composites, hindering the diffusion of oxygen and transfer of heat [16]. In addition, Chen et al. studied the effect of Cu₂O on the smoke suppression performance of EP composites containing ammonium polyphosphate (MAPP). Their results showed that Cu₂O could effectively reduce the production of smoke, which was due mainly to the fact that Cu₂O could promote the formation of a compact char layer during the combustion process. The compact char layer had the effect of impeding the exchange of heat and isolating oxygen [17]. In view of the above-mentioned findings, copper molybdate (CuMoO₄) was selected in the present work to modify h-BN because it contained two elements of molybdenum and copper. It was expected that loading CuMoO₄ on the surface of h-BN could not only improve the flame retardancy of the polymer more effectively, but also significantly improve its smoke suppression performance.

Polyurethane elastomer (PUE) is widely used for various products, such as sporting goods, toys and decorative materials, because of its good abrasion resistance, oil resistance and elasticity [18–20]. Unfortunately, PUE can rapidly burn and generate large amounts of harmful volatile substances and smoke while it is continuously heated [21, 22]. As a result, it is very important to effectively improve the flame retardancy and smoke suppression performance of PUE to expand the range of its application.

In this work, a green flame retardant (CuMoO₄@h-BN hybrid) was prepared by the co-precipitation method, and the application of CuMoO₄@h-BN in PUE was studied. The effects of CuMoO₄@h-BN on the flame retardancy and smoke suppression performance of PUE were investigated by using TGA, cone calorimeter and smoke density. Moreover, the flame retardant and smoke suppression mechanism were studied by the analysis of char residue after the cone calorimeter test.

Experimental

Materials

CuCl₂·2H₂O, Na₂MoO₄·2H₂O, H₂SO₄ (98%) were purchased from Sinopharm Chemical Reagent Co., Ltd., China. HNO₃ was purchased from Shanghai Yihai Chemical Reagent Co., Ltd., China. h-BN was

purchased from Weifang Ruida Ceramic Materials Co., Ltd., China. Polyester alcohol (Mn = 1975) was purchased from Shandong Xin Dezhou Huarun Polyurethane Industry Co., Ltd., China. 3,3'-Dichloro-4,4'-diaminodiphenylmethane (MOCA) was purchased from Jinan Haiwu Chemical Co., Ltd., China; Toluene diisocyanate (TDI) was purchased from Mitsui Chemical Co., Ltd., Japan.

Preparation of CuMoO_4 @h-BN

First, in order to improve the surface inertia and poor wettability, h-BN was treated with H_2SO_4 and HNO_3 [12]. h-BN was added into the mixed solution of H_2SO_4 and HNO_3 and then sonicated 5 h to generate a sticky and pale yellow suspended solution. After that, it was transferred to a four-necked flask, and the oil bath was refluxed at 80°C for 72 h. Finally, the supernatant was neutralized by washing with deionized water and then freeze-dried to obtain surface-functionalized h-BN, referred to as a-BN.

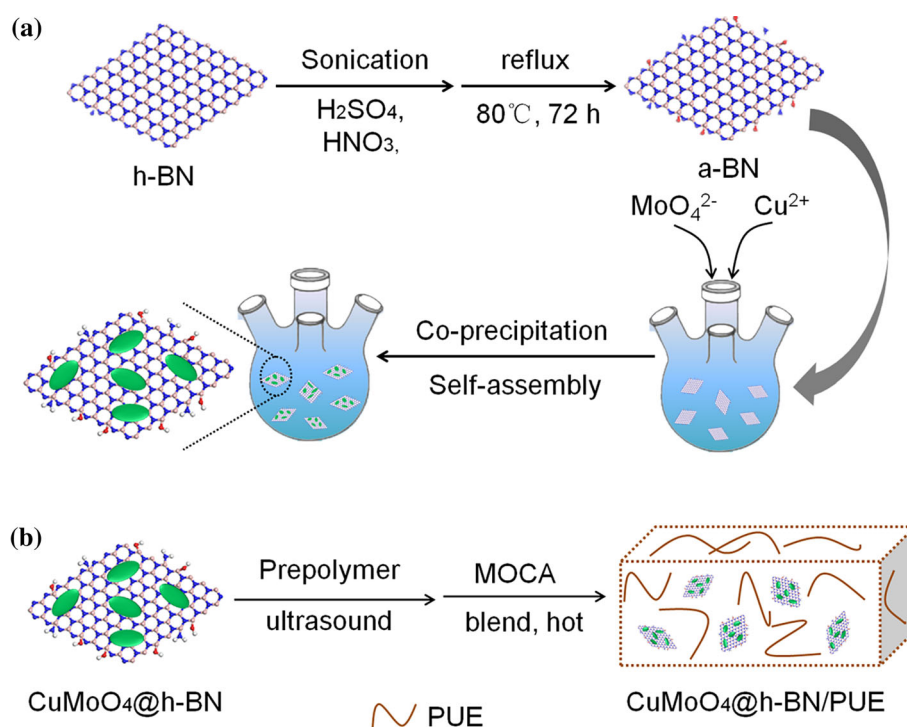
CuMoO_4 @h-BN was prepared as follows: First, 0.25 g a-BN was sonicated in 50 ml of deionized water for 30 min. Then, 0.171 g $\text{CuCl}_2 \cdot 2\text{H}_2\text{O}$ was dissolved in deionized water and added dropwise to the above liquid of a-BN with continued ultrasonic agitation for 1 h. The mixture was transferred to a four-necked flask, with oil bath at 60°C for 12 h.

Then, 0.242 g $\text{Na}_2\text{MoO}_4 \cdot 2\text{H}_2\text{O}$ aqueous solution was added dropwise to the above mixture with continued stirring for 2 h. After standing for a few hours, the supernatant was removed and then washed with deionized water. Finally, the above was freeze-dried to obtain a green CuMoO_4 @h-BN (0.48 g).

Preparation of PUE composites

PUE composites were prepared by simple blending. Typically, the PUE composite containing 2 wt% CuMoO_4 @h-BN was prepared as follows: Polyester polyol (44.4 g) was heated to 110°C , stirred, and vacuumed for 2 h to remove trace water. Then, polyester polyol was cooled to 70°C . TDI was added and stirred at 75°C for 2 h and then degassed under vacuum at 80°C for 30 min to obtain NCO group-terminated prepolymer. CuMoO_4 @h-BN (1 g) was dispersed into acetone by ultrasonication, poured into the prepolymer and stirred under ultrasound at 75°C to form a homogeneous mixture. Then, molten MOCA (4.6 g) was added into the above blend and stirred fully. Thereafter, the mixture was casted on a Teflon mold at 80°C for 8 h and placed in an oven at 120°C for 2 h. Finally, the PUE/ CuMoO_4 @h-BN composite was prepared. Pure PUE, PUE/h-BN and PUE/h-BN/ CuMoO_4 composites were prepared via a similar procedure. The filler loading of PUE/h-BN was kept at

Scheme 1 Illustration for the modification of h-BN and preparation of PUE composites.



2 wt%. The fillers of PUE/h-BN/CuMoO₄ were 1 wt% h-BN and 1 wt% CuMoO₄ (Scheme 1).

Characterization

X-ray diffraction (XRD) patterns were performed with a Bruker D8 X-ray diffractometer (Germany). Fourier transform infrared (FTIR) spectra were carried out with a Nicolet 6700 FTIR spectrophotometer (Thermo Fisher Scientific, USA). Laser Raman spectroscopy (LRS) measurements were taken with a SPEX-1403 laser Raman spectrometer (SPEX Co., USA). X-ray photoelectron spectroscopy (XPS) was performed with an ESCALAB 250 spectrometer (Thermo Scientific Ltd., USA). Transmission electron microscope–energy-dispersive X-ray spectroscopy (TEM-EDS) images were obtained using a JEM-2100 instrument (JEOL Co., Japan). Thermogravimetric analysis (TGA) was carried out on a Q50 thermo-analyzer instrument (TA Instruments, USA) under an air flow of 20 °C min⁻¹. Differential scanning calorimetry (DSC) was performed on a Q20 (TA Instruments, USA) from 20 to 150 °C at a linear heating rate of 20 °C min⁻¹. The cone calorimeter combustion test was performed on a JCZ-2 cone calorimeter (Jiangning Analytical Instrument Company, China) following the procedures given in the ISO5660 standard with heat radiation of 50 kW m⁻², and the size of each specimen was 100 × 100 × 4 mm³. The smoke density test was carried out in a JSC-2 smoke density test chamber (Jiangning Analytical Instrument Company, China) according to ISO 5659-2 with heat radiation of 50 kW m⁻², and the size of each specimen was 75 × 75 × 3 mm³.

Results and discussion

Characterization of CuMoO₄@h-BN

XRD is known to be a useful technique to examine the structure of inorganic materials. Figure 1 shows the XRD patterns of h-BN, CuMoO₄ and CuMoO₄@h-BN. As shown in the figure, the characteristic absorption peak of h-BN appears at 26.6°, 41.4°, 43.5°, 49.9°, 54.9° and 75.8° corresponding to (002), (100), (101), (102), (004) and (110) plane diffraction peaks, respectively [23]. The diffraction peaks of CuMoO₄ in the XRD pattern conform to the standard CuMoO₄

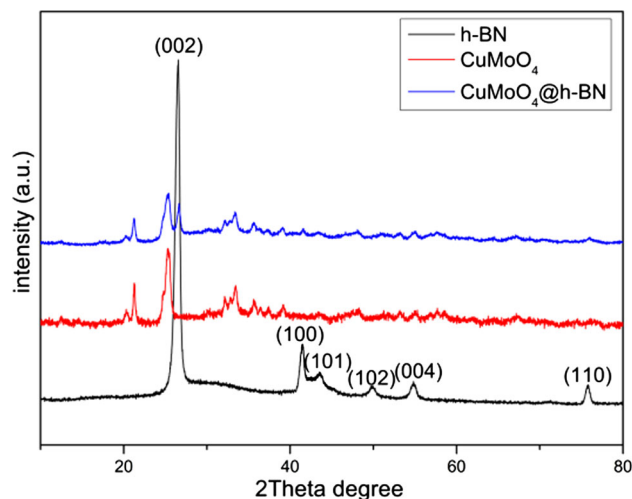


Figure 1 XRD patterns of as-prepared samples.

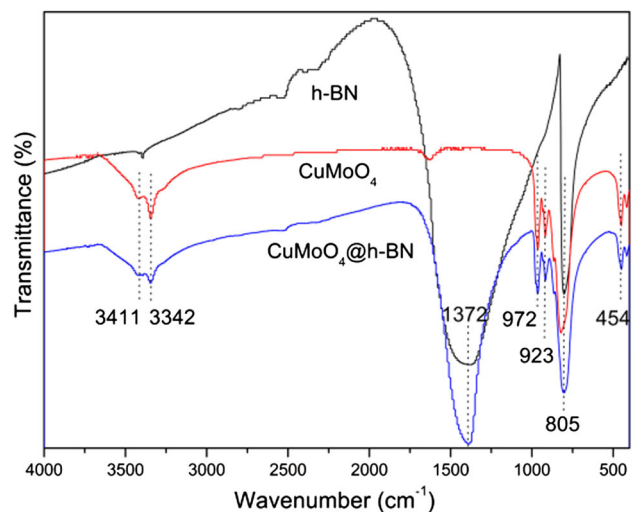


Figure 2 FTIR spectra of as-prepared samples.

diffraction peaks [24]. Compared with CuMoO₄ and h-BN, the diffraction peaks of CuMoO₄ and h-BN appear in the XRD spectrum of CuMoO₄@h-BN, indicating that CuMoO₄ is successfully supported on the surface of h-BN.

Figure 2 shows the FTIR spectra of h-BN, CuMoO₄ and CuMoO₄@h-BN. From the spectrum of h-BN, two obvious characteristic peaks are observed: the stretching vibration peak of B–N (1372 cm⁻¹) and the deformation vibration peak of B–N (805 cm⁻¹), which are typical of h-BN absorption peaks [25]. From the spectrum of CuMoO₄, two obvious absorption peaks can be observed between 3300 and 3500, which are the stretching vibration peak of O–H in adsorbed water and the stretching vibration peak of Mo = O at

Figure 3 TEM images of a h-BN; b CuMoO₄@h-BN; c EDS analysis of CuMoO₄@h-BN.

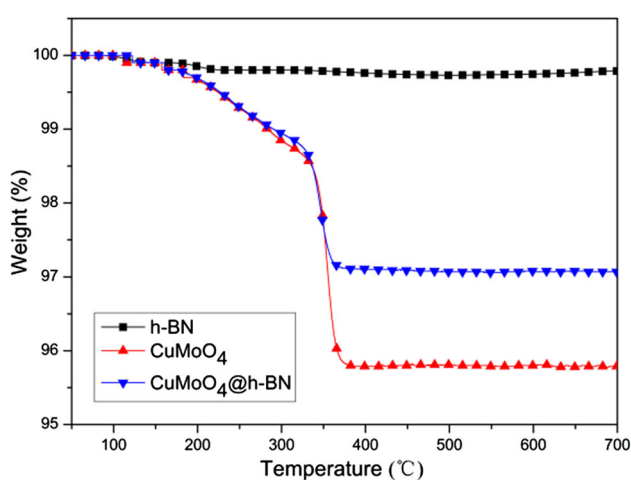
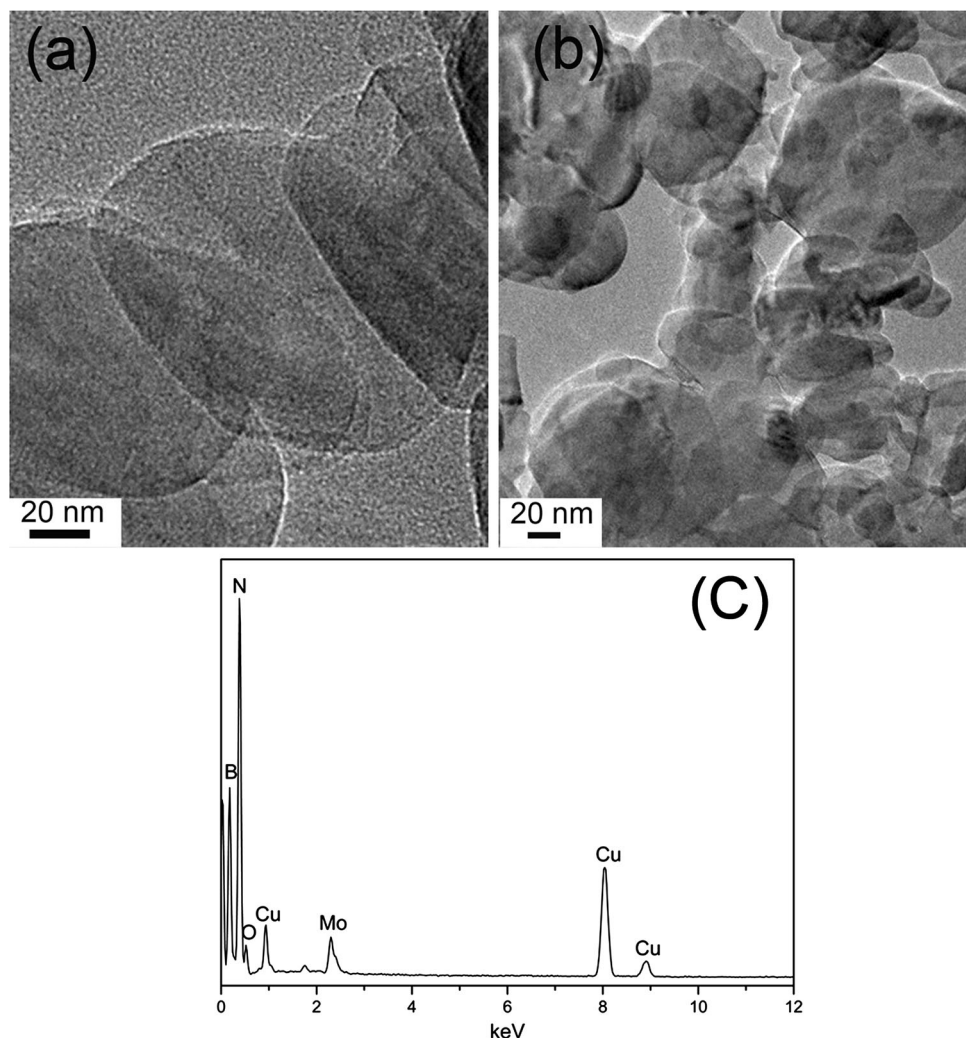


Figure 4 TGA curves of h-BN, CuMoO₄ and CuMoO₄@h-BN. 972 cm⁻¹, the stretching vibration peak of Mo-O-Mo at 815 cm⁻¹ and the absorption peak of Cu-O bond at 454 cm⁻¹ [26]. Compared with h-BN and CuMoO₄,

almost all absorption peaks of h-BN and CuMoO₄ are observable in the CuMoO₄@h-BN spectra, indicating that the hybrid of CuMoO₄@h-BN has been successfully prepared.

TEM is used to further study the morphology and composition of CuMoO₄@h-BN. Figure 3a shows that h-BN nanosheets are round or oval, stacked on top of each other, and their size is relatively uniform, about 100 nm. In Fig. 3b, we can see that a lot of CuMoO₄ sheets appear on the surface of h-BN, indicating that CuMoO₄ is loaded on the sheets of h-BN. The elemental composition of CuMoO₄@h-BN is obtained from Fig. 3c. It is clear that the B and N elements belong to the h-BN nanosheet. Cu, Mo and O all belong to CuMoO₄, while C belongs to the carbon film on the stage. EDS results further confirm that CuMoO₄@h-BN has been prepared.

Figure 4 presents the TGA curves of h-BN, CuMoO₄ and CuMoO₄@h-BN treated for 2 h in a

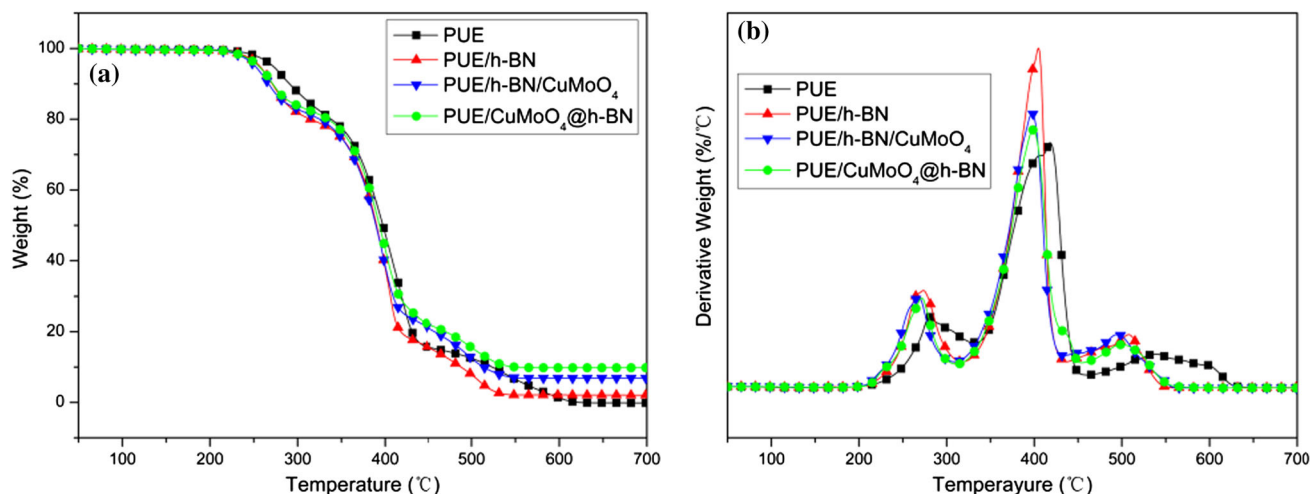


Figure 5 TGA (a) and DTG (b) curves of pure PUE and PUE composites.

vacuum oven at 60 °C. It can be seen from the figure that there is almost no mass change in h-BN, and the residual is as high as 99.8% at 700 °C, indicating the excellent thermal stability of h-BN. For CuMoO_4 , there is almost no mass loss before 150 °C. After 150 °C, the weight loss is due to the decomposition of CuMoO_4 into CuO and MoO_3 , and the residual is 95.7% at 700 °C. The weight loss trend of CuMoO_4 @h-BN is similar to that of CuMoO_4 , and the residual at 700 °C is obviously higher than that of CuMoO_4 , reaching 97.1%.

The thermal properties of pure PUE and its composites

Thermogravimetric analysis is used to investigate the thermal stability of pure PUE and its composites. Figure 5 shows the TGA and DTG curves for pure PUE, PUE/h-BN, PUE/h-BN/ CuMoO_4 and PUE/ CuMoO_4 @h-BN composites under air atmosphere. As can be seen from the figure, all the samples show a similar tendency of thermal decomposition under air conditions. First of all, the first decomposition occurs below 350 °C, which is mainly the process of hard segment decomposition to produce isocyanates, polyols and volatile materials. Then, a second decomposition takes place between 350 and 470 °C, which is attributed mainly to the decomposition of soft segments. Finally, there is a third decomposition after 470 °C, which is due to the degradation of metastable char.

As shown in Fig. 5, $T_{5\%}$ of pure PUE (corresponding to a sample with a mass loss of 5 wt%) is

275.4 °C and T_{\max} (corresponding to a maximum thermal decomposition rate) is 384.2 °C. Compared with pure PUE, there is a slight decrease in the $T_{5\%}$ of PUE/h-BN/ CuMoO_4 and PUE/ CuMoO_4 @h-BN composites. It is probably because that the metal oxides generated during the decomposition of CuMoO_4 catalyze the degradation of PUE [27]. The slight increase in the T_{\max} of PUE/h-BN/ CuMoO_4 and PUE/ CuMoO_4 @h-BN composites is attributed to the physical barrier effect of h-BN and char residue. In addition, the residual char yield of pure PUE is less than 0.1% at 700 °C, while those of PUE/h-BN, PUE/h-BN/ CuMoO_4 and PUE/ CuMoO_4 @h-BN are 2.1, 6.9 and 9.8%, respectively. It is noteworthy that the PUE/ CuMoO_4 @h-BN composite exhibits the most significant increase in its yield of char residue, which may be attributed to a better barrier effect with better dispersibility of h-BN and a catalytic carbonization effect from the metal oxides produced by the decomposition of CuMoO_4 @h-BN (Table 1).

In general, the glass transition temperature (T_g) is an important parameter to characterize thermal properties of polymers and is frequently used to represent the segmental mobility of macromolecular chains. The T_g of PUE and its composites are characterized by DSC, and the results are shown in Fig. 6. Compared with pure PUE, the T_g of the PUE composites are all increased in some degrees. It may be because the physical barrier effect of h-BN and CuMoO_4 helps hinder the movement of molecular chains to a certain extent [28].

Table 1 Data of TGA and DTG of pure PUE and PUE composites

Sample	$T_{10\%}$ (°C)	T_{max} (°C)	Residue at 700 °C (%)
PUE	275.4	384.2	< 0.1
PUE/h-BN	256.7	403.9	2.1
PUE/h-BN/CuMoO ₄	251.6	397.4	6.9
PUE/CuMoO ₄ @h-BN	255.1	399.2	9.8

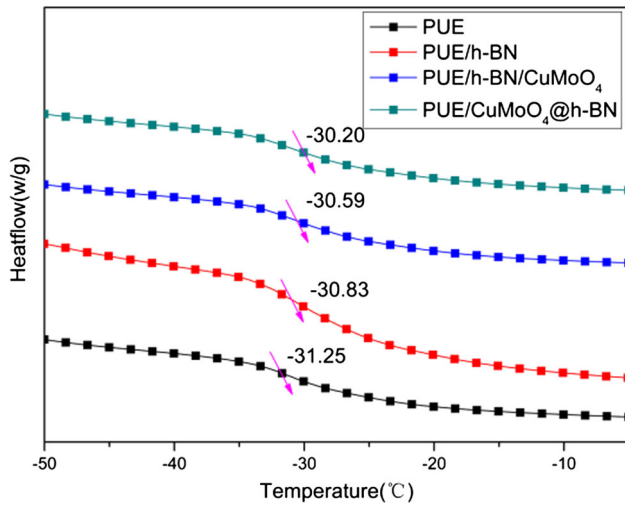


Figure 6 DSC thermograms of pure PUE and PUE composites.

The flame retardancy of pure PUE and its composites

Figure 7 shows the heat release rate (HRR) and total heat release (THR) curves of pure PUE and its composites. The related data are shown in Table 2. As can be seen from the figure, pure PUE can ignite rapidly in combustion, with a peak heat release rate (PHRR) of 1106 kW m⁻² and total heat release (THR) of 61.7 MJ m⁻². Compared with pure PUE, the PHRR and THR of PUE/h-BN, PUE/h-BN/CuMoO₄ and PUE/CuMoO₄@h-BN are all decreased to some extent. Among them, the PHRR and THR of PUE/CuMoO₄@h-BN are decreased most obviously, by 73.6 and 52.4%, respectively. This is due mainly to the physical barrier effect between the h-BN nanosheets and the char layer produced during the combustion

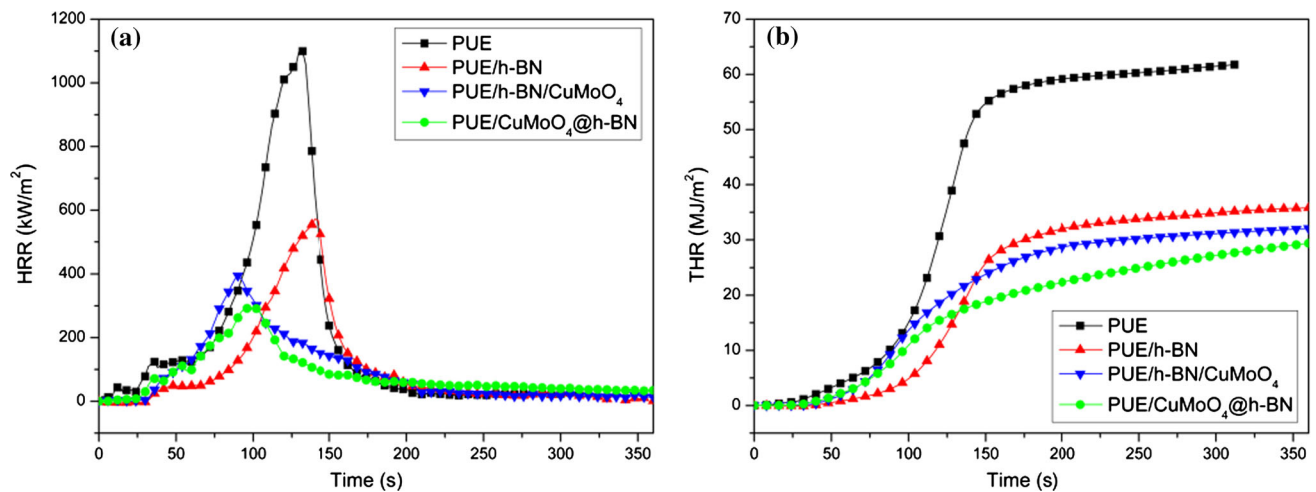


Figure 7 HRR (a) and THR (b) curves of pure PUE and PUE composites.

Table 2 PHRR, THR, SPR and TSP data of pure PUE and PUE composites

Sample	PHRR (KW/m ²)	THR (MJ/m ²)	SPR (m ² /s)	TSP (m ²)	Mass (%)
PUE	1106	61.7	0.144	8.9	4.3
PUE/h-BN	571	35.8	0.103	8.8	12.3
PUE/h-BN/CuMoO ₄	394	32.2	0.07	8.2	19.5
PUE/CuMoO ₄ @h-BN	292	29.4	0.06	8.5	24.4

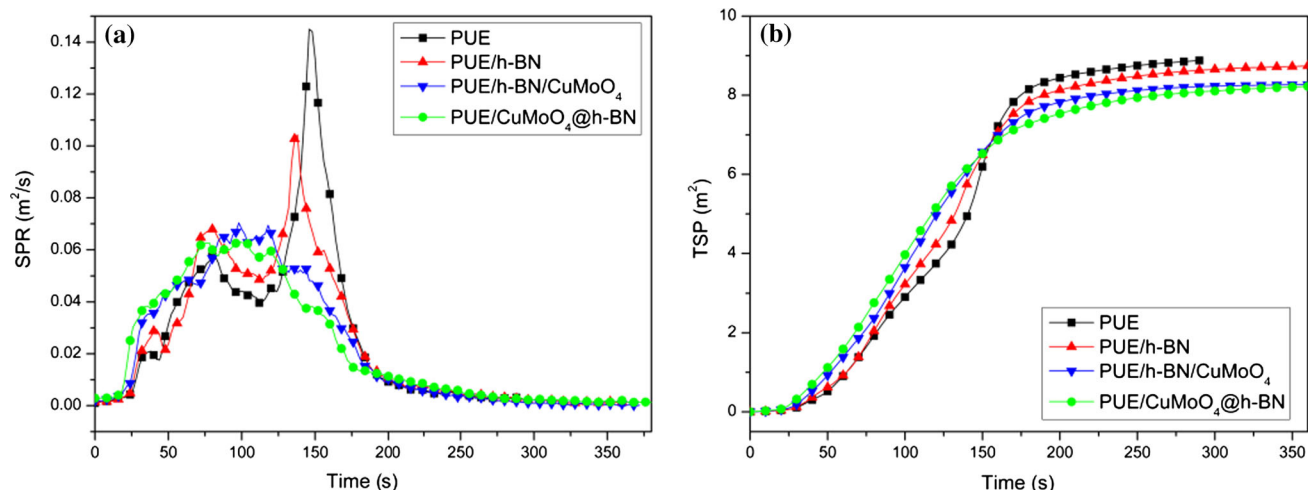


Figure 8 SPR (a) and TSP (b) curves of pure PUE and PUE composites.

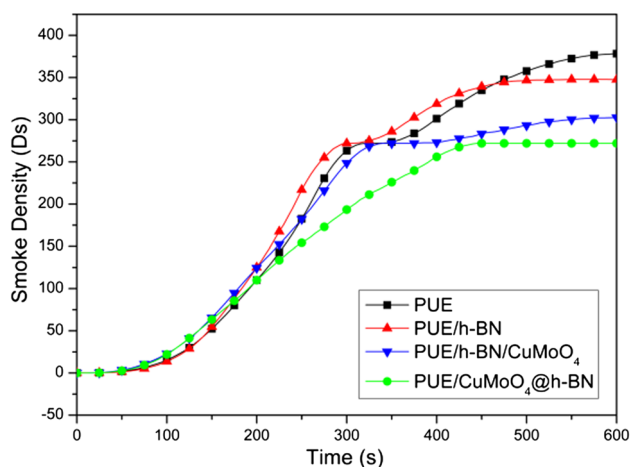


Figure 9 Smoke density curves of pure PUE and PUE composites.

Table 3 Smoke density data of pure PUE and PUE composites

Sample	^a $D_{s,10}$	^b $D_{s,max}$
PUE	379	379
PUE/h-BN	349	349
PUE/h-BN/CuMoO ₄	303	303
PUE/CuMoO ₄ @h-BN	272	272

^a $D_{s,max}$ the maximum value of smoke density

^b $D_{s,10}$ the value of smoke density at 600 s

process, suppressing the volatilization of the flammable gas generated during the decomposition of the polymer, isolating oxygen and reducing heat radiation. Meanwhile, CuMoO₄ can decompose and generate Cu₂O and MoO₃ during the heating process. Cu₂O and MoO₃ have the function of catalyzing the

formation of a compact char layer [16, 29]. More compact char layers can produce a better physical barrier effect, thereby enhancing the flame retardancy of the composite.

Smoke suppression performance of pure PUE and PUE composites

The smoke generation rate (SPR) and the total smoke generation (TSP) are two important parameters in the cone calorimetry test to assess the smoking behavior of polymers during combustion. Figure 8 shows the SPR and TSP curves for the cone calorimetric test of PUE and its composites. The SPR and TSP of pure PUE reach 0.14 m² s⁻¹ and 8.9 m², respectively. When different flame retardants are added, the SPR and TSP of the composites all decrease to some degrees. Among them, the SPR and TSP of PUE/CuMoO₄@h-BN are decreased most, indicating that CuMoO₄@h-BN has a better smoke suppression effect. This is because that, on the one hand, the physical barrier effect of h-BN is in play; on the other hand, Cu₂O and MoO₃ generated during the decomposition of CuMoO₄ have a catalytic carbonization effect, enhancing the densification of the residual char and suppressing the combustion of the material, thereby reducing the release of smoke.

The smoke density test under flameless combustion conditions is used to further investigate the influence of CuMoO₄@h-BN on the smoke suppression performance of PUE. The results are shown in Fig. 9 and Table 3. Pure PUE has the largest smoke density value at 600 s compared with the PUE

composites. When 2 wt% h-BN is added, the smoke density of PUE/h-BN is 349, only 7.9% lower than that of pure PUE. Such a slight reduction in smoke density may be attributed to the barrier effect of h-BN. Meanwhile, it shows that the barrier effect is not strong in smoke suppression. The smoke density of PUE/h-BN/CuMoO₄ is decreased to 303 at 600 s and that of PUE/CuMoO₄@h-BN is decreased to 272 at 600 s. It indicates that CuMoO₄ loaded on the surface of h-BN has a more active smoke suppression effect, which is consistent with the cone calorimetric test results.

Char residue analysis of PUE and its composites

Figure 10 presents the char residue mass curves of PUE and its composites after the cone calorimeter test. As can be seen from the figure, the char yield of pure PUE is 11.4%. The char yield of the PUE composites is all increased after the addition of different flame retardants. Notably, the char yield of PUE/CuMoO₄@h-BN is increased most obviously, indicating that CuMoO₄@h-BN has a better effect of catalytic carbonization. This result is consistent with the TGA test results.

Figure 11 displays the digital photographs of PUE and its composites after the cone calorimeter test. They intuitively show that pure PUE has a little residual char after combustion. It is worth noting that the residual char of PUE/CuMoO₄@h-BN is thicker. It is attributed mainly to the physical barrier effect of CuMoO₄@h-BN and the catalytic carbonization effect

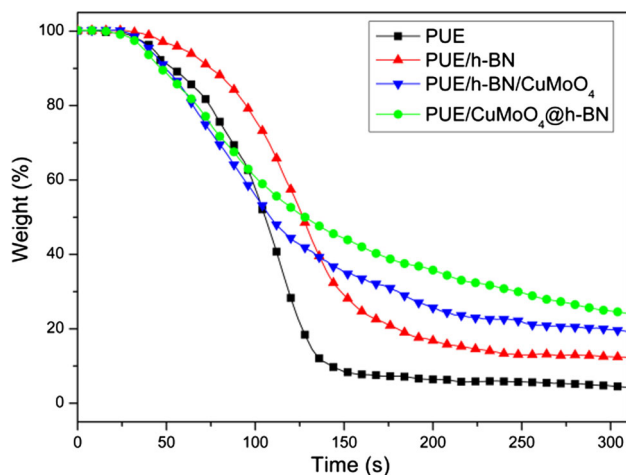


Figure 10 Char residue mass curves of PUE and its composites after cone calorimeter test.

of its decomposed metal oxides. It is consistent with the results of the TGA test.

The Raman spectra of the char residue of PUE and its composites after the cone calorimeter test are shown in Fig. 12. It can be seen from the figure that the Raman spectra of the four samples have a similar shape, with two peaks at 1360 and 1600 cm⁻¹, which correspond to D and G band (D band represents the symmetrical carbon atoms of amorphous carbon vibration, and G band represents two-dimensional sp² hybrid graphite carbon atoms in the symmetrical stretching vibration), respectively. The graphitization degree of char can be estimated by the relative intensity ratio of the D and G bands (I_D/I_G). The lower the ratio of I_D/I_G , the higher the graphitization degree of the char [30, 31]. The I_D/I_G value of pure PUE is 4.35. In comparison, the I_D/I_G values of PUE/h-BN, PUE/h-BN/CuMoO₄ and PUE/CuMoO₄@h-BN all decrease to some extent. Among them, PUE/CuMoO₄@h-BN has the smallest I_D/I_G value, which indicates that CuMoO₄@h-BN can effectively promote the formation of graphitized carbon, improving the graphitization degree of residual char, thereby enhancing the flame retardancy and smoke suppression performance of PUE.

Figure 13 shows the C 1 s spectra of PUE and its composites after the cone calorimeter test, with the corresponding data listed in Table 4. The thermal oxidation resistance of polymer is investigated by calculating the C_{ox}/C_a value (C_{ox} : oxidized carbons and C_a : aliphatic and aromatic carbons). The smaller the value of C_{ox}/C_a , the higher the thermal oxidation resistance of the composite formed during the combustion process [32]. The char layer with high thermal oxidative resistance could effectively inhibit the heat and mass transfer between the flame and matrix, delay the degradation of inner polymer and thus retard the combustion. As listed in Table 4, the C_{ox}/C_a value of pure PUE is 0.86. Those of PUE/h-BN and PUE/h-BN/CuMoO₄ are reduced to 0.75 and 0.66, respectively. However, the C_{ox}/C_a value of PUE/CuMoO₄@h-BN is further decreased to 0.56, indicating that CuMoO₄@h-BN could effectively improve the thermal oxidation resistance of the char residue, and that PUE/CuMoO₄@h-BN has higher flame retardancy and smoke suppression properties.

Figure 14 shows the Mo 3d, Cu 2p_{3/2} and Cu LMM spectra of PUE/CuMoO₄@h-BN residual char after the cone calorimeter test. As shown in Fig. 14a, the Mo 3d peak can be fitted into three peaks. Two peaks

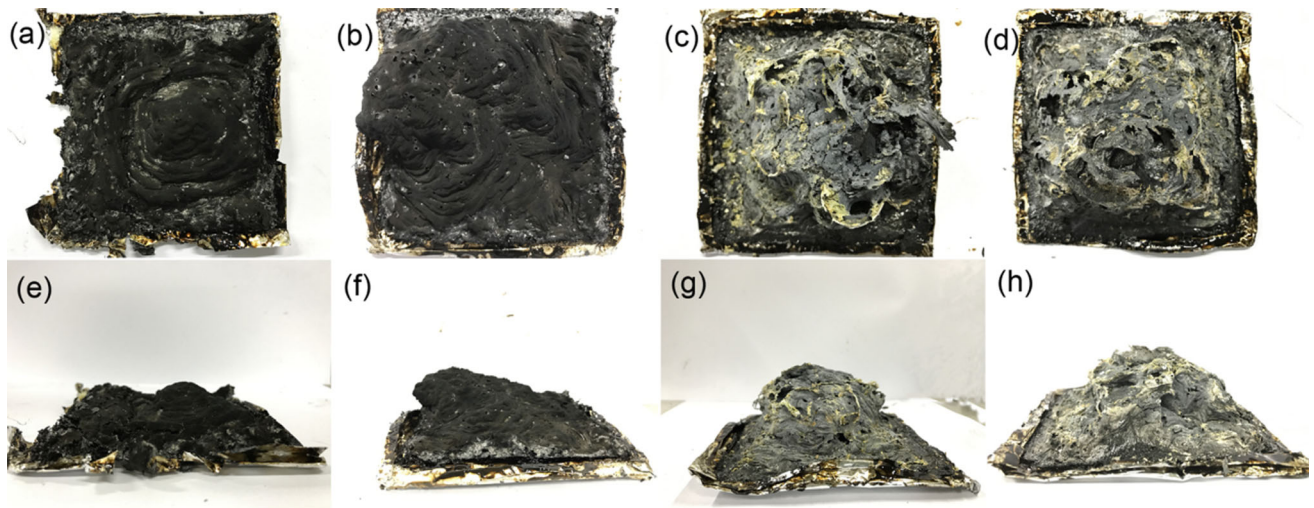


Figure 11 Digital photographs of the samples after cone calorimeter test: pure PUE (a, e), PUE/h-BN (b, f), PUE/h-BN/CuMoO₄ (c, g), PUE/CuMoO₄@h-BN (d, h).

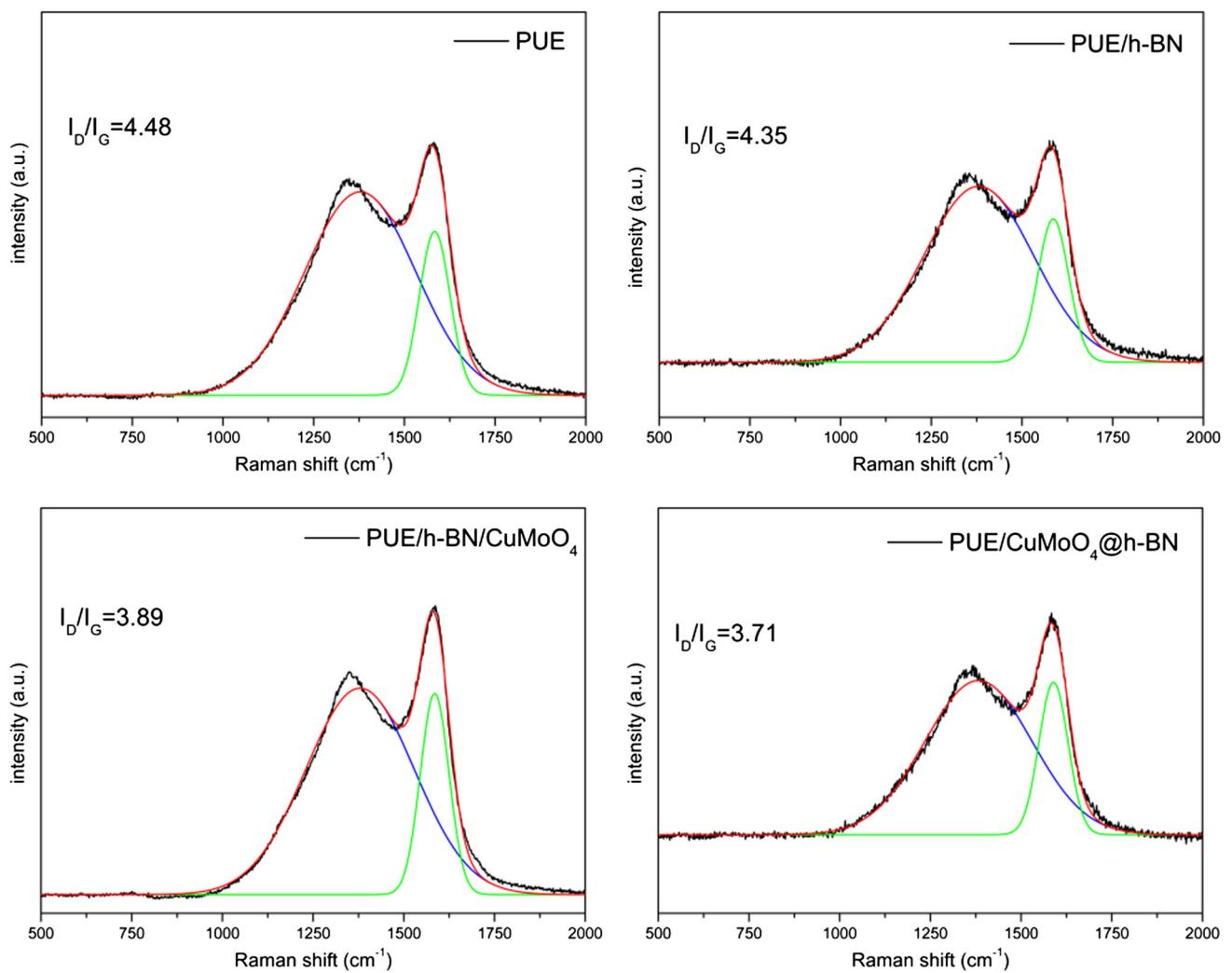


Figure 12 Raman spectra of char residue of pure PUE and PUE composites.

at 229.45 and 232.7 eV are attributed to the binding energies of $\text{Mo}^{4+} 3d_{5/2}$, $\text{Mo}^{4+} 3d_{3/2}$ and $\text{Mo}^{6+} 3d_{3/2}$, respectively, indicating that +4 and +6 valences of molybdenum compounds are present in the char residue of PUE/ CuMoO_4 @h-BN [33]. The Cu $2p_{3/2}$ peak is fitted to four peaks, and the two peaks at 934.5 and 932.8 eV belong to the binding energy of Cu^{2+} , Cu^+ or Cu^0 . In addition, there are two satellites of Cu^{2+} between the 938 and 945 eV peak (S1 and S2). Since the binding energies of Cu^+ and Cu^0 are extremely small in the Cu $2p_{3/2}$ spectrum, it is difficult to distinguish the existence of Cu^+ and Cu^0 . Therefore, the Auger (LMM) spectrum of Cu is used to distinguish the existence of Cu^+ and Cu^0 [34]. It can be seen that the Cu LMM peak can be fitted into three peaks belonging to Cu^0 , Cu^+ and Cu^{2+} , respectively, indicating that copper, +1 and +2

valence copper-containing compounds coexist in the residual char of the PUE/ CuMoO_4 @h-BN composite.

XRD is used to further analyze the residual char after the cone calorimeter test of PUE/ CuMoO_4 @h-BN to explore the types of Mo and Cu compounds. The results are shown in Fig. 15. The diffraction peak of h-BN can be seen in the figure, indicating that the residual char still contains h-BN. The h-BN sheet has good thermal stability and can play a very good role with a barrier effect in the polymer's combustion process. In addition, the diffraction peaks of MoO_3 and MoO_2 can also be found in the spectrum, as the result of thermal decomposition of CuMoO_4 . Among them, MoO_3 as a Lewis acid in the decomposition of the matrix through the promotion of Friedel–Crafts alkylation reaction to form more residual char

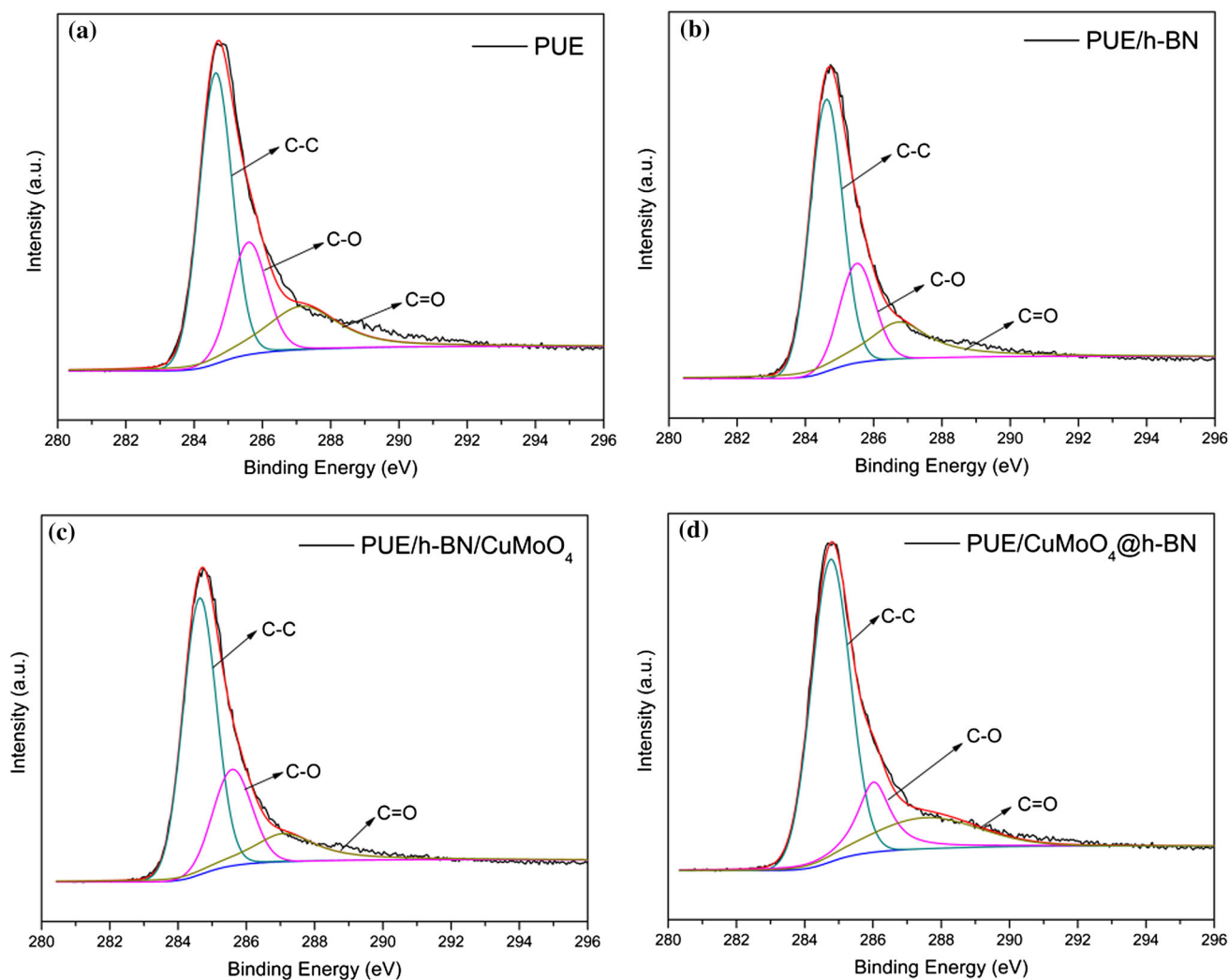


Figure 13 C 1s spectra of char residue of pure PUE and PUE composites.

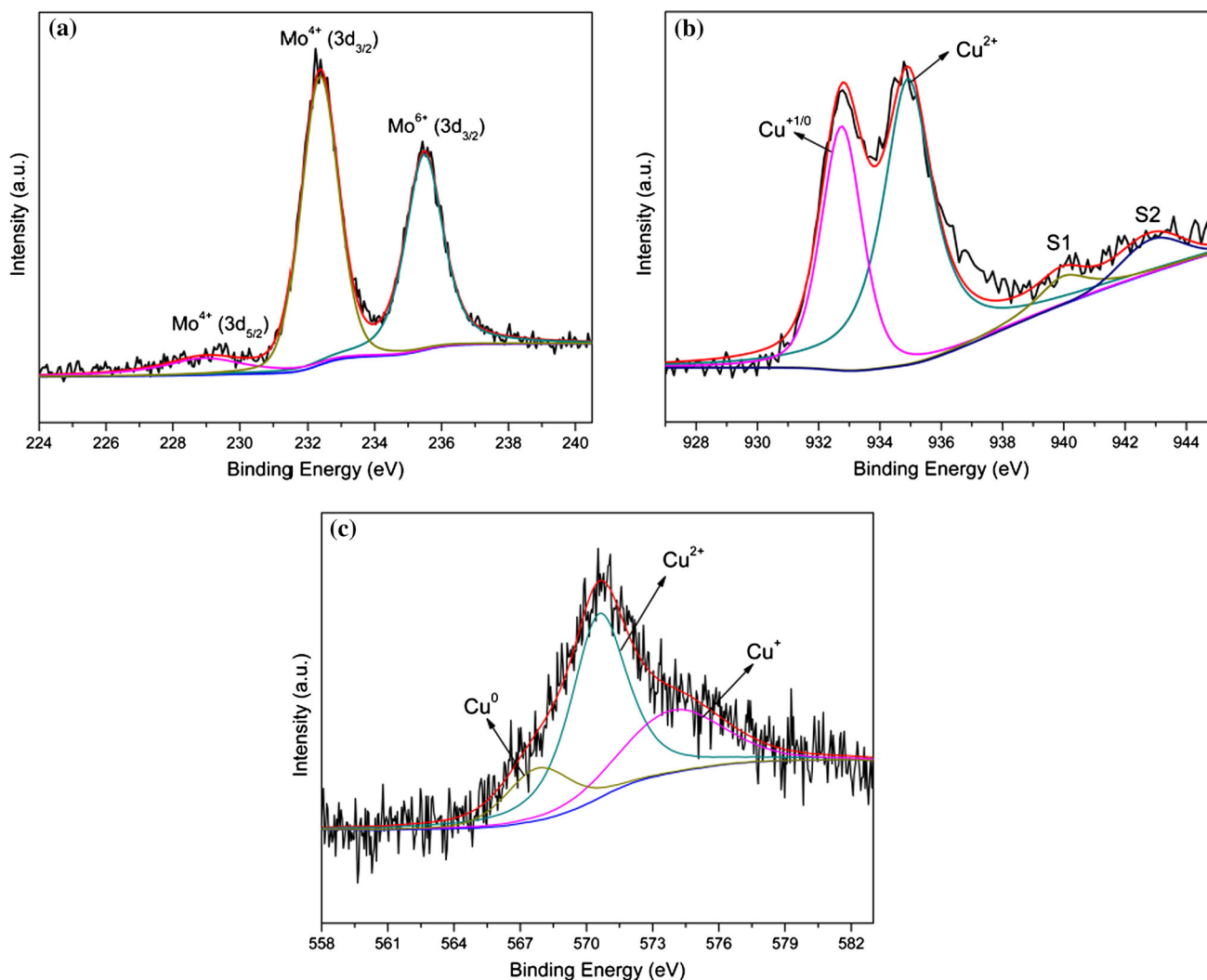
Table 4 Results of C 1s XPS of char residue of pure PUE and PUE composites

Samples	C–C Area (%)	C–O Area (%)	C=O Area (%)	C_{ox}/C_a
PUE	53.8	23.4	22.8	0.86
PUE/h-BN	56.9	22.0	21.1	0.75
PUE/h-BN/CuMoO ₄	59.9	23.8	16.3	0.66
PUE/CuMoO ₄ @h-BN	63.8	17.6	18.6	0.56

inhibits further combustion of the matrix [35]. In addition, Cu element in the residual char in the form of single element Cu, CuO and Cu₂O exists. Cu₂O can catalyze the coupling reaction between polymer molecular chains to form a continuous dense char layer. At the same time, Cu₂O can be reduced to

elemental Cu by reductive gases such as CO and H₂, and elemental Cu can be oxidized by oxygen to Cu₂O, thereby continuing to exert its catalytic carbonization effect, promoting the formation of more char residue and reducing the smoke emission of the polymer [36].

Based on the above, the mechanism of flame retardancy and smoke suppression properties of PUE/CuMoO₄@h-BN is illustrated in Scheme 2. The reason for the improved flame retardancy and smoke suppression of the PUE composite, on the one hand, is ascribed to the physical barrier effect of h-BN, and on the other hand, is that CuMoO₄ generates MoO₃ and Cu₂O during the combustion process. MoO₃ and Cu₂O have the effect of promoting the formation of a compact char layer. The compact char layer can effectively inhibit heat transfer in the system during

**Figure 14** Mo 3d (a), Cu 2p_{3/2} (b) and Cu LMM (c) spectra of char residue of PUE/CuMoO₄@h-BN.

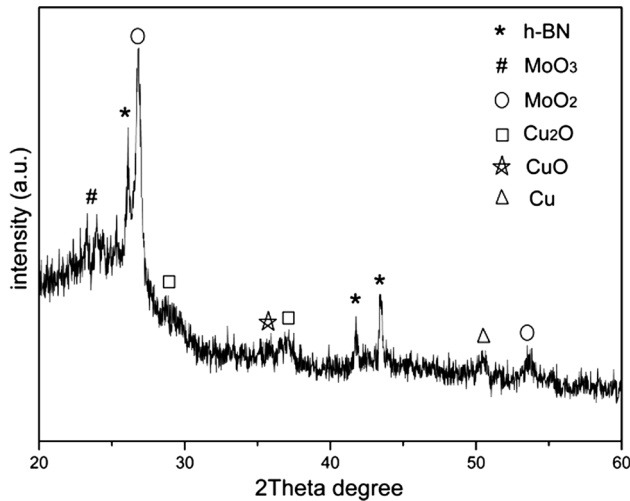


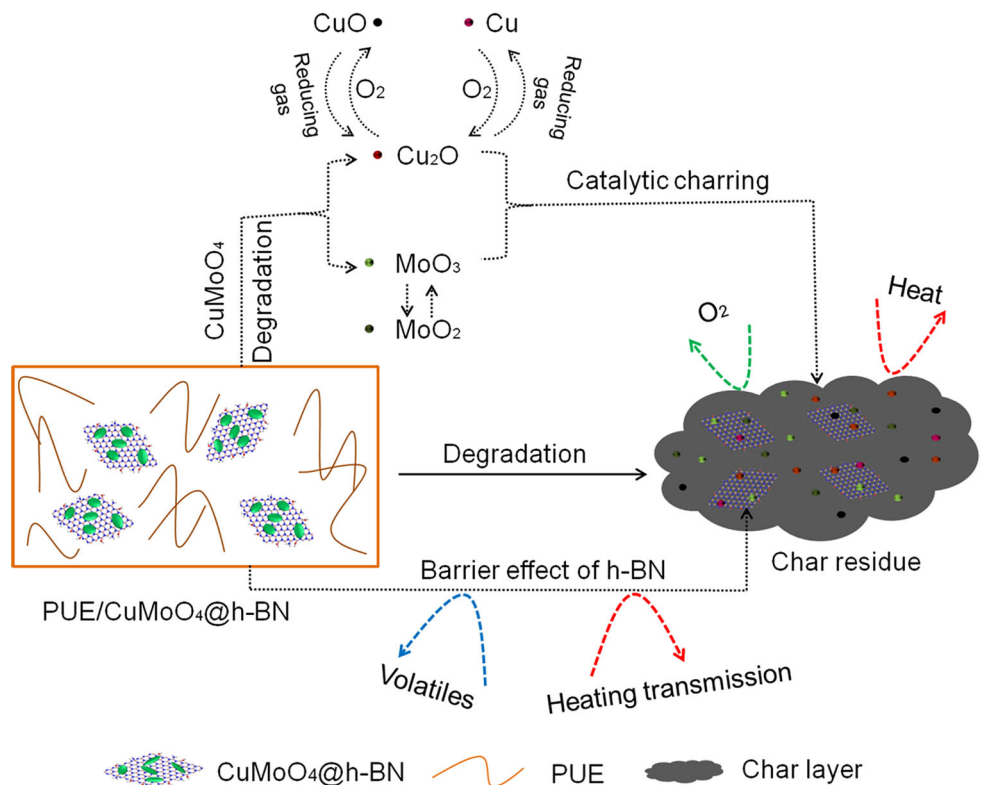
Figure 15 XRD pattern of the char residue after the cone calorimeter test of PUE/CuMoO₄@h-BN.

the combustion of the polymer, slow down the volatilization and diffusion of flammable gas and retard the further degradation of the composites.

Conclusions

In this work, CuMoO₄ was loaded on the surface of h-BN to synthesize a novel flame retardant (CuMoO₄@h-BN). The structure of CuMoO₄@h-BN was systematically characterized. Subsequently, CuMoO₄@h-BN was added to PUE to study the influence of CuMoO₄@h-BN on its thermal, flame retardancy and smoke suppression properties. The results of TGA showed that the char yield of PUE/CuMoO₄@h-BN reached 9.8% at 700 °C, indicating that CuMoO₄@h-BN had a good effect of catalytic carbonization. In addition, the PHRR, THR and *D_{s,max}* of CuMoO₄@h-BN/PUE decreased by 73.6, 52.4 and 28.2%, respectively. CuMoO₄@h-BN exhibited an excellent flame retardancy and smoke suppression performance. CuMoO₄@h-BN could improve the flame retardancy and smoke suppression properties of PUE due to the physical barrier effect of h-BN and the catalytic charring effect of CuMoO₄. The char layer acted as a physical barrier, inhibiting the exchange of heat between the fire and the matrix, isolating O₂, and thereby retarding the further degradation of the polymer. Hopefully, the approach demonstrated herein will be a promising pathway for improving the flame retardancy and

Scheme 2 Schematic illustration of the flaming PUE/CuMoO₄@h-BN.



smoke suppression properties of polymer composites.

Acknowledgements

The authors are grateful to the Anhui Provincial Natural Science Foundation (1708085ME113), the Natural Science Research Project of Colleges and Universities in Anhui Province (KJ2018A0522) and Polymer Materials and Engineering Specialty Comprehensive Reform Pilot Project in College Quality Engineering Project of Anhui Province (2016zy031) for their financial support.

Compliance with ethical standards

Conflict of interest The authors declare that they have no conflict of interest.

References

- [1] Holder KM, Smith RJ, Grunlan JC (2017) A review of flame retardant nanocoatings prepared using layer-by-layer assembly of polyelectrolytes. *J Mater Sci* 52:12923–12959 <https://doi.org/10.1007/s10853-017-1390-1>
- [2] Jian R, Wang P, Xia L, Yu X, Zheng X, Shao Z (2017) Low-flammability epoxy resins with improved mechanical properties using a Lewis base based on phosphaphenanthrene and 2-aminothiazole. *J Mater Sci* 52:1–15 <https://doi.org/10.1007/s10853-017-1102-x>
- [3] Kandola BK, Ebdon JR, Luangtriratana P, Krishnan L (2016) Novel flame retardant thermoset resin blends derived from a free-radically cured vinylbenzylated phenolic novolac and an unsaturated polyester for marine composites. *Polym Degrad Stab* 127:56–64
- [4] Jin X, Gu X, Chen C, Tang WF, Li HF, Liu XD, Bourbigot S, Zhang ZW et al (2017) The fire performance of polylactic acid containing a novel intumescent flame retardant and intercalated layered double hydroxides. *J Mater Sci* 52:12235–12250 <https://doi.org/10.1007/s10853-017-1354-5>
- [5] Shen KK, Kochesfahani S, Jouffret F (2010) Zinc borates as multifunctional polymer additives. *Polym Adv Technol* 19:469–474
- [6] Wicklein B, Kocjan D, Carosio F, Bergström L (2016) Tuning the nanocellulose-borate interaction to achieve highly flame retardant hybrid materials. *Chem Mater* 28:1985–1989
- [7] Tran TT, Elbadawi C, Totonjian D, Lobo CJ, Grosso G, Moon H, Englund DR, Michael JF et al (2016) Robust multicolor single photon emission from point defects in hexagonal boron nitride. *ACS Nano* 10:7331–7338
- [8] Jungwirth NR, Calderon B, Ji Y, Spencer MG, Flatte ME, Fuchs GD (2016) Temperature dependence of wavelength selectable zero-phonon emission from single defects in hexagonal boron nitride. *Nano Lett* 16:6052–6057
- [9] Weng Q, Wang X, Wang X, Bando Y, Golberg D (2016) Functionalized hexagonal boron nitride nanomaterials: emerging properties and applications. *Chem Soc Rev* 45:3989–4012
- [10] Yu B, Xing WY, Guo WW, Qiu SL, Wang X, Lo S, Hu Y (2016) Thermal exfoliation of hexagonal boron nitride for effective enhancements on thermal stability, flame retardancy and smoke suppression of epoxy resin nanocomposites via sol-gel process. *J Mater Chem A* 4:7330–7340
- [11] Jin WQ, Yuan L, Liang GZ, Gu AJ (2014) Multifunctional cyclotriphosphazene/hexagonal boron nitride hybrids and their flame retarding bismaleimide resins with high thermal conductivity and thermal stability. *ACS Appl Mater* 6:14931–14944
- [12] Qu TG, Yang N, Hou J, Li GH, Yao YM, Zhang QX, He LQ, Wu DZ et al (2017) Flame retarding epoxy composites with poly(phosphazene-co-bisphenol A)-coated boron nitride to improve thermal conductivity and thermal stability. *RSC Adv* 7:6140–6151
- [13] Xu W, Li C, Hu Y, Liu L, Hu Y, Wang P (2016) Synthesis of MoO₃ with different morphologies and their effects on flame retardancy and smoke suppression of polyurethane elastomer. *Polym Adv Technol* 27:964–972
- [14] Hou Y, Hu W, Gui Z, Hu Y (2017) Effect of cuprous oxide with different sizes on thermal and combustion behaviors of unsaturated polyester resin. *J Hazard Mater* 334:39–48
- [15] Zhou K, Gao R, Qian X (2017) Self-assembly of exfoliated molybdenum disulfide (MoS₂) nanosheets and layered double hydroxide (LDH): towards reducing fire hazards of epoxy. *J Hazard Mater* 338:343–355
- [16] Xu WZ, Liu L, Zhang BL, Hu Y, Xu BL (2016) Effect of molybdenum trioxide-loaded graphene and cuprous oxide-loaded graphene on flame retardancy and smoke suppression of polyurethane elastomer. *Ind Eng Chem Res* 55:4930–4941
- [17] Chen MJ, Lin YC, Wang XN, Zhong L, Li QL, Liu ZG (2015) Influence of cuprous oxide on enhancing the flame retardancy and smoke suppression of epoxy resins containing microencapsulated ammonium polyphosphate. *Ind Eng Chem Res* 54:12705–12713
- [18] Bourbigot S, Samyn F, Turf T, Duquesne S (2010) Nanomorphology and reaction to fire of polyurethane and polyamide nanocomposites containing flame retardants. *Polym Degrad Stab* 95:320–326

- [19] Sheng D, Tan J, Liu X, Wang P, Yang Y (2011) Effect of organoclay with various organic modifiers on the morphological, mechanical, and gas barrier properties of thermoplastic polyurethane/organoclay nanocomposites. *J Mater Sci* 46:6508–6517 <https://doi.org/10.1007/s10853-011-5597-2>
- [20] Chen KY, Kuo JF (2002) Surface characterization and platelet adhesion studies of aliphatic polyurethanes grafted by fluorocarbon oligomers: effect of fluorocarbon chain length and carboxylic acid group. *J Mater Sci Mater Med* 13:37–45 <https://doi.org/10.1023/A:1013678301050>
- [21] Dike AS, Tayfun U, Dogan M (2017) Influence of zinc borate on flame retardant and thermal properties of polyurethane elastomer composites containing huntite-hydro-magnesite mineral. *Fire Mater* 41:890–897
- [22] Chen X, Wang W, Jiao C (2017) A recycled environmental friendly flame retardant by modifying para-aramid fiber with phosphorus acid for thermoplastic polyurethane elastomer. *J Hazard Mater* 331:257–264
- [23] Mahdizadeh A, Farhadi S, Zabardasti A (2017) Microwave-assisted rapid synthesis of graphene-analogue hexagonal boron nitride (h-BN) nanosheets and their application for the ultrafast and selective adsorption of cationic dyes from aqueous solutions. *RSC Adv* 7:53984–53995
- [24] Rahimi-Nasrabadi M, Pourmortazavi SM, Khalilian-Shalamzari M (2015) Facile chemical synthesis and structure characterization of copper molybdate nanoparticles. *J Mol Struct* 1083:229–235
- [25] Goldin N, Dodiuk H, Dan L (2017) Enhanced thermal conductivity of photopolymerizable composites using surface modified hexagonal boron nitride fillers. *Compos Sci Technol* 152:36–45
- [26] Shahri Z, Salavati-Niasari M, Mir N, Kianpour G (2014) Facile synthesis and characterization of nanostructured flower-like copper molybdate by the co-precipitation method. *J Cryst Growth* 386:80–87
- [27] Xu WZ, Zhang BL, Wang XL, Wang GS, Ding D (2017) The flame retardancy and smoke suppression effect of a hybrid containing CuMoO_4 , modified reduced graphene oxide/layered double hydroxide on epoxy resin. *J Hazard Mater* 343:364–375
- [28] Zhou KQ, Liu JJ, Shi YQ, Jiang SH, Wang D, Hu Y, Gui Z (2015) MoS_2 nanolayers grown on carbon nanotubes: an advanced reinforcement for epoxy composites. *ACS Appl Mater Interfaces* 7:6070–6081
- [29] Wang B, Zhou KQ, Wang BB, Gui Z, Hu Y (2014) Synthesis and characterization of $\text{CuMoO}_4/\text{Zn-Al}$ layered double hydroxide hybrids and their application as a reinforcement in polypropylene. *Ind Eng Chem Res* 53:12355–12362
- [30] Yuan BH, Hu Y, Chen XF, Shi YQ, Niu Y, Zhang Y, He S, Dai HM (2017) Dual modification of graphene by polymeric flame retardant and Ni(OH)_2 nanosheets for improving flame retardancy of polypropylene. *Compos Part A Appl Sci* 100:106–117
- [31] Hou YB, Hu W, Gui Z, Hu Y (2017) Bi_2Se_3 nanosheets: advanced nanofillers for reinforcing and flame retarding polyethylene nanocomposites. *Compos Part A Appl Sci* 100:71–380
- [32] Bourbigot S, Bras ML, Delobel R, Gengembre L (1997) XPS study of an intumescent coating: II. Application to the ammonium polyphosphate/pentaerythritol/ethyleneic terpolymer fire retardant system with and without synergistic agent. *Appl Surf Sci* 120:15–29
- [33] Kobe B, Badley M, Henderson JD, Anderson S, Biesinger MC, Shoesmith D (2017) Application of quantitative X-ray photoelectron spectroscopy (XPS) imaging: investigation of Ni–Cr–Mo alloys exposed to crevice corrosion solution. *Surf Interface Anal* 49:1345–1350
- [34] Liu P, Hensen EJ (2013) Highly efficient and robust $\text{Au/MgCuCr}_2\text{O}_4$ catalyst for gas-phase oxidation of ethanol to acetaldehyde. *J Am Chem Soc* 135:14032–14035
- [35] Cai W, Zhan J, Feng XM, Yuan BH, Liu JJ, Hu WZ, Hu Y (2017) Facile construction of flame-retardant-wrapped molybdenum disulfide nanosheets for properties enhancement of thermoplastic polyurethane. *Ind Eng Chem Res* 56:7229–7238
- [36] Tu HB, Wang JQ (1996) An XPS investigation of thermal degradation and charring processes for PVC and PVC/ Cu_2O systems in the condensed phase-II. *Polym Degrad Stab* 54:195–203